ACADEMIC PRESS

Available online at www.sciencedirect.com

SCIENCE DIRECT®

Journal of Sound and Vibration 263 (2003) 21–46

JOURNAL OF SOUND AND VIBRATION

www.elsevier.com/locate/jsvi

# High-frequency vibration analysis of thin elastic plates under heavy fluid loading by an energy finite element formulation

Weiguo Zhang[a], Aimin Wang[a], Nickolas Vlahopoulos[a,*], Kuangcheng Wu[b]

[a] *Department of Naval Architecture and Marine Engineering, University of Michigan, 2600 Draper Rd., Ann Arbor, MI 48109-2145, USA*

[b] *Signatures and Hydrodynamics, Northrop Grumman Newport News, 4101 Washington Ave., Newport News, VA 23607-2770, USA*

Received 29 August 2001; accepted 8 June 2002

**Abstract**

An energy finite element analysis (EFEA) formulation for computing the high frequency behavior of plate structures in contact with a dense fluid is presented. The heavy fluid loading effect is incorporated in the derivation of the EFEA governing differential equations and in the computation of the power transfer coefficients between plate members. The new formulation is validated through comparison of EFEA results to classical techniques such as statistical energy analysis (SEA) method and the modal decomposition method for bodies of revolution. Good correlations are observed and the advantages of the EFEA formulation are identified.



## 1. Introduction

It is often necessary to compute high-frequency vibration of marine structures that are in contact with a dense fluid. This information can be useful in designing marine vehicles that exhibit reduced acoustic signatures and self-noise characteristics, and for reducing interior noise levels in passenger and crew compartments. In the past an energy finite element analysis (EFEA) formulation has been developed for computing the vibration of larger scale dry structures and marine vehicles at high frequencies [1–3]. The EFEA developments were validated by comparing numerical EFEA results to available test data, by comparing EFEA solutions with results computed by very dense conventional finite element models, and by comparing EFEA results to

*Corresponding author. Tel.: +1-734-764-8341; fax: +1-734-936-8820.
*E-mail address:* nickvl@engin.umich.edu (N. Vlahopoulos).

0022-460X/03/$ - see front matter 
doi:10.1016/S0022-460X(02)01096-9

statistical energy analysis (SEA) results. In this paper, a new development to account for fluid loading in the existing EFEA formulation is presented. Considerable work has been performed for the dynamic and acoustic response of plates under heavy fluid loading [4–17]. Generally, below the coincidence frequency the fluid effect is expressed as added mass while radiation into the fluid occurs only by the edges and the corners of a finite plate. Several models are available in the literature for evaluating the radiation efficiency below the coincidence frequency [8,18–20]. Above coincidence frequency the fluid loading effect is represented only in terms of the radiation damping [5,21]. In this paper, an EFEA formulation for thin elastic plates in contact with a heavy fluid is presented and validated. Only the exterior fluid loading on one side of plates is considered here. The EFEA has been developed recently for high-frequency structural/acoustic simulations [22–28] and constitutes an alternative formulation to the established SEA method. In EFEA, the primary variable is defined as the time and space averaged energy density. The governing differential equations are developed with respect to the energy density, and a finite element approach is employed for the numerical solution. The EFEA formulation was validated for analyzing dry marine structures through comparison of the EFEA results to experimental data and to SEA results [1]. Overall, the EFEA constitutes a wave approach for high-frequency analysis while the SEA is a modal approach. In previous work, the heavy fluid loading effect has not been included in the EFEA formulation.

The major stages in the evolution of analytical approaches for coupled fluid–structure interaction are summarized and discussed by Junger [29] and Crighton [30]. Junger [29] identified a number of milestones in the understanding of the fluid–structure interaction, such as the asymptotic evaluation of the far field for baffled, infinite planar, and cylindrical structures using stationary phase integration and inverse wavenumber transform. The explicit farfield solution of locally excited, radiation-loaded infinite plates and cylindrical shells was also overviewed [29]. Crighton [30] summarized the progress that has been made using complex integral transform techniques and methods of asymptotic singular perturbation theory in analytical developments.

Computational methods based on finite element and boundary element formulations have been developed for performing coupled fluid–structure computations [31]. Methods for modelling fluid effects are also available in some commercial finite element analysis (FEA) codes [32,33]. An approach for analyzing complex structures under heavy fluid loading by employing a combination of analytical and FEA techniques was also presented [34]. It was suggested that fluid-loaded, nearly planar large structural elements can be treated as structures in a vacuum with equivalent material properties. Then the equivalent structure could be analyzed by FEA techniques [34].

In high frequencies, when the dimension of the structure is large with respect to the wavelength, FEA-based methods become infeasible. SEA is a mature and established approach for high-frequency structural/acoustic analysis [35–38]. In SEA, a vibro-acoustic system is divided into subsystems of similar modes. The lumped averaged energy within each subsystem of similar modes comprises the primary SEA variable and the power transferred between subsystems is expressed in terms of coupling loss factors. Crighton [30] discussed some aspects of incorporating heavy fluid loading effects into SEA. Resonance frequencies and mode shapes that included the effect of fluid loading were utilized in defining the dynamics of the corresponding subsystems. The influence of the heavy fluid loading on coupling loss factor across a rib between two plates was investigated [39,40]. It was demonstrated that fluid loading tends to mend the discontinuity introduced by a rib in a panel. The mending is expressed in terms of an increase in the

transmission efficiency across the rib. In SEA the power transferred from structural subsystems to an acoustic is expressed in terms of the radiation efficiency. Very early efforts were made in identifying properly the radiation efficiency below the coincidence frequency. The radiation efficiency was determined by several factors, such as the plate dimensions, the material properties of the plate and the fluid, and the excitation [41]. The effect of the fluid loading on the acoustic radiation from an infinite plate subjected to a point or to a line force or moment excitation was identified [5]. The radiation and the transmission across simple line supports of steel plates with water on one side was discussed in Ref. [6]. The acoustic power radiated by thin panels excited by turbulent-boundary-layer wall pressure was estimated by a modal method and employed in an SEA application [8]. A precise mathematical formulation for the acoustic radiation efficiency of a rectangular panel was developed [19]. An alternative method for determining numerically the radiation efficiency for point excited plates was published [20]. The new approach was employed in SEA computations for underwater noise radiated from ship hulls and the calculations were compared favorably to test data. For light damped plates and a reverberant vibration field, the radiation from the flexural near field around the excitation point was demonstrated to be negligible [20,41]. In mid- and high-frequency range, the modal density within a considered frequency band is high. The analytical expressions for the radiation efficiency averaged over a frequency band were derived for plates with high modal densities [8,18,19].

In this paper, the added mass effect of the heavy fluid loading and the radiation damping effect are incorporated in the existing EFEA formulation for dry structures for computing the high-frequency vibration of structures comprised by thin plates in contact with a heavy fluid on one side. The procedure is similar to the manner suggested by Crighton [30] for incorporating the heavy fluid loading effect in an SEA formulation. The plate equations under fluid loading [21] are employed for defining a basis of orthogonal waves in the plate. The orthogonal waves constitute a basis for expressing the behavior of the plate similar to the modal basis employed in the definition of each SEA subsystem. The energy associated with the response of a plate is derived by adding incoherently the energy of the orthogonal waves of the basis [2,42,43]. Thus, an energy density variable comprises the primary variable of the EFEA similar to the energy of a subsystem being the primary variable in SEA. The intensity of the response of a plate is also derived in a similar manner as resultant from incoherent orthogonal waves. A relationship between the energy density and the intensity is derived by considering their expressions in terms of the orthogonal waves [2,3]. From the power balance over a control volume, the relationship between energy density and intensity, and the relationship between energy density and dissipated power, the EFEA governing differential equation is formulated in terms of the energy density. A finite element approach is employed for producing the numerical system of equations. The heavy fluid effect and the radiation damping are included in the derivation process by using the effective mass and the total damping factor in the EFEA governing differential equation. The total damping factor includes both structural and radiation damping. The frequency averaged radiation efficiency model from Ref. [19] is employed in this EFEA formulation. The effective mass is employed for deriving the radiation damping from the radiation efficiency, similar to the approach presented in Ref. [20].

The primary variable of the EFEA is discontinuous at joints between components. Power transfer coefficients are utilized for coupling the energy density across a joint. A formulation for power transfer coefficients of plates under heavy fluid loading is also developed. The method presented in Ref. [44] for computing power transfer coefficients between plates at joints is

modified in order to take into account that some of the members at a joint can be in contact with heavy fluid. The power transfer coefficients are evaluated from analytical solutions of semi-infinite members that demonstrate the same structural characteristics with the members for which the power transfer coefficients are computed. The heavy fluid loading effect is included in the derivation of the power transfer coefficients by modifying appropriately the flexural wavenumbers of the members which are in contact with heavy fluid.

The validity of the new EFEA formulation that includes the heavy fluid loading effect is demonstrated by comparing EFEA solutions to results obtained by classical techniques such as the SEA and the modal decomposition method for bodies of revolution. Comparison of the EFEA results with data from a very dense conventional FEA model is also included in this validation. A plate in contact with water on one side, a cylindrical structure immersed into water and a small undersea vehicle are analyzed. The comparison is performed over a frequency range where the modal decomposition method, the EFEA method, and the SEA method are valid.

## 2. Overview of vibration characteristics of a thin plate under heavy fluid loading

The equations associated with the vibration of a thin plate under heavy fluid loading are summarized first. They are employed for defining the basis of orthogonal waves used in the derivation of the EFEA governing differential equation. Considering an infinite thin plate under heavy fluid loading (Fig. 1), the in-plane and the flexural displacement are not coupled and the fluid motion is only coupled with the flexural displacement. The governing equation of motion for the flexural displacement is [21,30]

$$D(1+\mathrm{i}\eta_{damp})\nabla^4 w + m\frac{\partial^2 w}{\partial t^2} = -p_{z=0}, \tag{1}$$

where $D$ is the bending stiffness of the plate, $\eta_{damp}$ is the structural damping factor, $m=\rho_s h$ is the plate surface mass density, ($\rho_s$ is the plate mass density and $h$ is the plate thickness), and $p_{z=0}$ is the pressure exerted by the fluid on the vibrating plate. For steady state conditions, the amplitude $P$ of the pressure $p_{z=0}$ is a solution to the Helmholtz equation

$$(\nabla^2 + k^2)P = 0, \tag{2}$$

where $k$ is the acoustic wavenumber. For an infinite plate, an expression for the farfield solution of the flexural displacement of Eq. (1) in the $x$ direction is [21]

$$w = W\mathrm{e}^{-\mathrm{i}\gamma x}\mathrm{e}^{\mathrm{i}\omega t}, \tag{3}$$

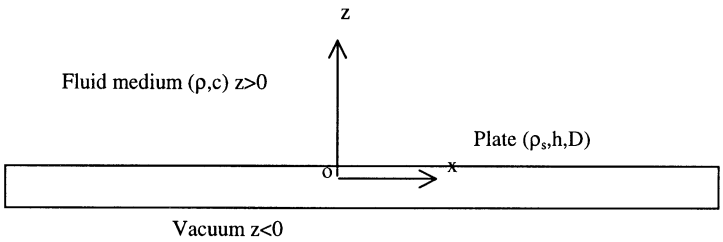


Fig. 1. Free Vibration of an infinite thin elastic plate exposed to heavy fluid loading from one side.

where $\gamma$ is defined as the flexural wavenumber of a plate under fluid loading, and $W$ is the wave amplitude. Similarly, a farfield solution for the pressure in Eq. (2) is

$$P = p_0 e^{ik_x x} e^{ik_z z}, \tag{4}$$

where $p_0$ is defined as the pressure at the origin, $k_x$, $k_z$ are the components of the acoustic wavenumber in the $x$ and $z$ directions. The wave expressions in Eqs. (3) and (4) include only farfield terms because at high frequencies the dimension of the plate is considerably larger than the wavelength and any near field effects are considered negligible. The sound field is linked to the structural wave motion through a boundary condition requiring that the normal component of the acceleration is continuous at the interface between the fluid and the structure:

$$\frac{1}{\rho}\frac{\partial p}{\partial z} = i\omega\frac{\partial w}{\partial t}, \tag{5}$$

where $\rho$ is the fluid mass density. The dispersion relation is obtained from Eqs. (1) to (5):

$$D(1 + i\eta_{damp})\gamma^4 - m\omega^2 - \frac{\omega^2\rho}{i\sqrt{k^2 - \gamma^2}} = 0, \tag{6}$$

where $\gamma$ is a solution to Eq. (6). A valid approximate solution for $\gamma$ is obtained by introducing $\gamma = k_f$ in the denominator of the third term in Eq. (6) [21], where $k_f$ is the flexural wavenumber of a plate in vacuum and $k_f = \sqrt[4]{(m/D)\omega^2}$. Therefore, Eq. (6) can be rewritten as

$$D(1 + i\eta_{damp})\gamma^4 - m\omega^2 - \frac{\omega^2\rho}{i\sqrt{k^2 - k_f^2}} = 0. \tag{7}$$

The nature of the solution to Eq. (7) depends on the relative value between $k$ and $k_f$. If $k < k_f$, then the vibration frequency is below the coincidence frequency, and the solution is

$$\gamma = \sqrt[4]{\frac{m}{D(1 + i\eta_{damp})}\omega^2\left(1 + \frac{\rho}{m\sqrt{k_f^2 - k^2}}\right)} \tag{8}$$

The effective surface mass density can be defined as

$$m_{eff} = m\left(1 + \frac{\rho}{m\sqrt{k_f^2 - k^2}}\right). \tag{9}$$

By considering light structural damping, $\gamma$ can be approximated by a Taylor expansion from Eq. (8) as

$$\gamma \cong \sqrt[4]{\frac{m_{eff}}{D}\omega^2}\left(1 - i\frac{\eta_{damp}}{4}\right). \tag{10}$$

If $k > k_f$, the vibration frequency is above the coincidence frequency, and the solution for $\gamma$ is

$$\gamma = \sqrt[4]{\frac{m}{D(1+\mathrm{i}\eta_{damp})}\omega^2\left[1-\mathrm{i}\frac{\rho}{m\sqrt{k^2-k_f^2}}\right]}. \tag{11}$$

By defining the radiation damping factor as

$$\eta_{rad} = \frac{\rho}{m\sqrt{k^2-k_f^2}} \tag{12}$$

and assuming light structural damping, $\gamma$ can be approximated from Eq. (11) as

$$\gamma = \sqrt[4]{\frac{m}{D(1+\mathrm{i}\eta_{damp})}\omega^2[1-\mathrm{i}\eta_{rad}]} \cong \sqrt[4]{\frac{m}{D}\omega^2}\left[1-\mathrm{i}\frac{(\eta_{damp}+\eta_{rad})}{4}\right]. \tag{13}$$

The total damping factor is defined as the sum between structural damping and radiation damping, $\eta = \eta_{damp} + \eta_{rad}$, and Eq. (13) can be rewritten as

$$\gamma \cong \sqrt[4]{\frac{m}{D}\omega^2}\left[1-\mathrm{i}\frac{\eta}{4}\right]. \tag{14}$$

Eqs. (10) and (14) provide the expressions for the plate flexural wavenumber under heavy fluid loading at different frequency ranges. Since structural damping is considered, the flexural wavenumber is complex in both frequency ranges. When the frequency range is below the coincidence frequency, the effective surface mass density is employed instead of the dry surface mass density. When the frequency range is above the coincidence frequency, the total damping factor is used instead of the structural damping factor. Eqs. (10) and (14) reflected the heavy fluid effect on the plate vibration characteristics of an infinite plate. For a finite plate, acoustic energy radiates into the fluid even for frequencies below the coincidence frequency due to edge and corner effects [18]. Eq. (10) is modified to include the radiation effect for a finite plate. Andresen [20] recently presented a numerical method for determining the radiation damping factor for point excited plates with heavy fluid loading. Radiation parameters in an SEA analysis was used to compute the noise radiated from the hull of a ship, and the results had reasonable correlation to test data. The radiation coefficient for a 10 mm thick steel plate with dimensions equal to 0.6 m × 1.5 m was presented in Ref. [20]. The radiation coefficient for the same plate is evaluated by frequency averaged radiation efficiency models presented by Davies [8], Maidanik [18] and Leppington et al. [19]. The results are summarized in Fig. 2. The results by the Davies model and the Maidanik model are indistinguishable below ~1000 Hz. Based on these results, Leppington's model appears to agree better with the radiation damping presented in Ref. [20] and it is employed in this paper. The radiation from the flexural near field around the excitation point is small and neglected since high modal densities and light structural damping within the plate are considered in high-frequency vibration [20,41]. Below the coincidence frequency, the radiation efficiency from Leppington's model is

$$\sigma_{rad} = \frac{a+b}{\pi\mu kab(\mu^2-1)^{1/2}}\left\{\ln\left(\frac{\mu+1}{\mu-1}\right)+\frac{2\mu}{\mu^2-1}\right\}, \quad \mu > 1, \tag{15}$$

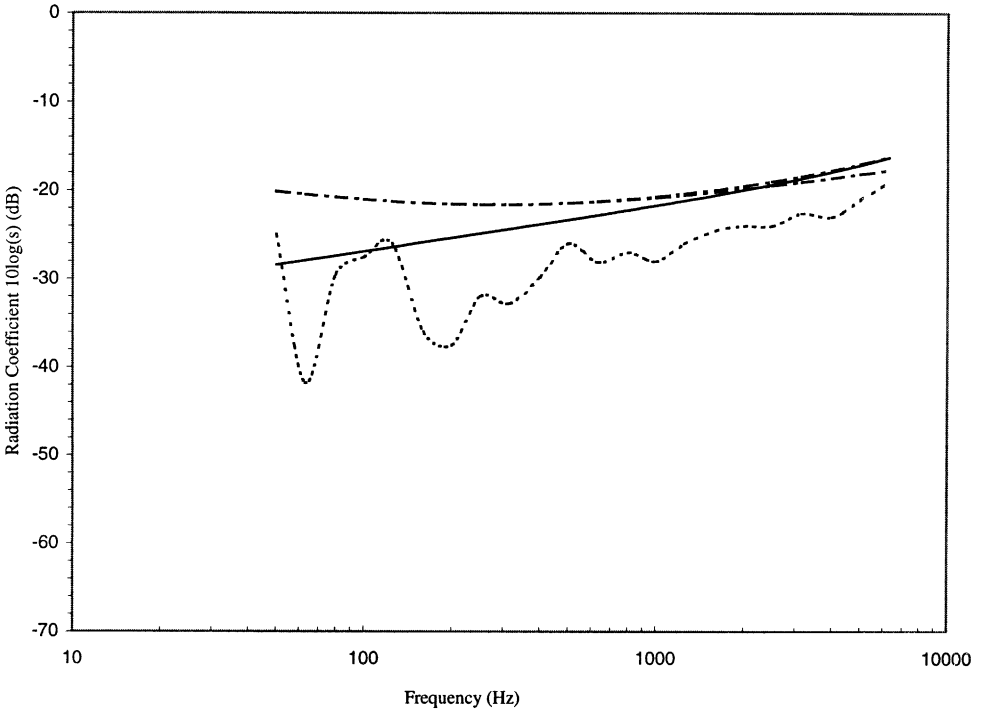


Fig. 2. Radiation coefficients computed by different analytical models for a 0.6 m × 1.5 m × 0.01 m steel plate in contact with water: ——, Leppington; - - - - -, Andresen; -·-·-, Maidanik; - · · - · · -, Davies.

where $a$ and $b$ are the length and width of the plate, $\mu = k_f/k$ is the wavenumber ratio. The radiation damping factor can be derived directly from radiation efficiency as $\eta_{rad} = (\rho c/(\omega m))\sigma_{rad}$. Considering the heavy fluid loading effect, Andresen [20] utilized the effective surface mass density of a plate for computing the radiation damping factor from the radiation efficiency. In a similar manner, in this work Eq. (15) is used to compute the radiation efficiency for a finite plate below coincidence frequency, and the radiation damping factor is evaluated using the effective surface mass density:

$$\eta_{rad} = \frac{\rho c}{\omega m_{eff}}\sigma_{rad}. \tag{16}$$

Therefore, for a finite plate, Eq. (10) is modified by including the radiation damping factor derived from Eq. (16):

$$\gamma \cong \sqrt[4]{\frac{m_{eff}}{D}\omega^2}\left(1 - \mathrm{i}\frac{\eta_{damp} + \eta_{rad}}{4}\right) = \sqrt[4]{\frac{m_{eff}}{D}\omega^2}\left(1 - \mathrm{i}\frac{\eta}{4}\right). \tag{17}$$

In summary, the effect of the heavy fluid loading below the coincidence frequency is expressed in terms of the effective surface mass density (Eq. (9)) and the radiation damping (Eqs. (16) and (17)). Above the coincidence frequency the fluid loading effect is expressed only in terms of the radiation damping factor defined in Eq. (14).

## 3. Development of the energy finite element formulation of finite thin plates under heavy fluid loading

### 3.1. Derivation of the energy governing equation for finite thin plates under heavy fluid loading

The flexural displacement of a finite thin plate under heavy fluid loading can be considered as a linear superposition of waves associated with any two orthogonal directions $x$ and $y$ [2,3]:

$$w_x = (A_x e^{-i\gamma_x x} + B_x e^{i\gamma_x x}) e^{i\omega t}, \tag{18}$$

$$w_y = (A_y e^{-i\gamma_y y} + B_y e^{i\gamma_y y}) e^{i\omega t} \tag{19}$$

where $A_x$, $A_y$, $B_x$, $B_y$ are constants associated with the waves in $x$ and $y$ directions, $\gamma_x$ and $\gamma_y$ are the complex flexural wavenumbers of the plate under fluid loading,

$$\gamma_x = \gamma_{x1}\left(1 - i\frac{\eta}{4}\right), \quad \gamma_y = \gamma_{y1}\left(1 - i\frac{\eta}{4}\right) \tag{20}$$

and

$$\gamma_{x1} = \gamma_{y1} = \sqrt[4]{\frac{m_{eff}}{D}\omega^2}, \quad \eta = \eta_{damp} + \eta_{rad}. \tag{21}$$

An expression for the energy density and the intensity is derived for each one of the two orthogonal waves. The derivation associated with the wave in the $x$ direction is discussed in detail. The corresponding energy variables for the $y$ direction are derived in a similar manner. The time averaged over a period energy density and intensity are expressed in terms of the displacement:

$$\langle e_x \rangle = \frac{D}{4}\left[\frac{\partial^2 w_x}{\partial x^2}\left(\frac{\partial^2 w_x}{\partial x^2}\right)^* + \frac{m_{eff}}{D}\frac{\partial w_x}{\partial t}\left(\frac{\partial w_x}{\partial t}\right)^*\right], \tag{22}$$

$$\langle I_x \rangle = \frac{D}{2}\mathrm{Re}\left[\frac{\partial^2 w_x}{\partial x^2}\left(\frac{\partial^2 w_x}{\partial x \partial t}\right)^* + \frac{\partial^3 w_x}{\partial x^3}\left(\frac{\partial w_x}{\partial t}\right)^*\right]. \tag{23}$$

In Eq. (22) the effective surface mass density is used for considering the added mass effect due to the heavy fluid when computing the energy density. The wave equation (18) is introduced into Eqs. (22) and (23). Neglecting higher order damping terms, and space averaging over a wavelength results in

$$\langle \underline{e}_x \rangle = \frac{D}{4}\left[\left(\gamma_{x1}^4 + \frac{m_{eff}}{D}\omega^2\right)(A_x^2 e^{-(\eta/2)\gamma_{x1}x} + B_x^2 e^{(\eta/2)\gamma_{x1}x})\right], \tag{24}$$

$$< \underline{I}_x >= D\gamma_{x1}^3 \omega (A_x^2 e^{-(\eta/2)\gamma_{x1}x} - B_x^2 e^{(\eta/2)\gamma_{x1}x}). \tag{25}$$

The time averaged over a period and space averaged over a wavelength energy density and intensity of the flexural waves constitute the primary energy variables of the EFEA plate formulation. The energy density and the intensity associated with the $y$ direction are expressed by a similar set of equations.

The vibration of the plate is considered as incoherent since at high frequencies the flexural wavelength is small compared to the dimension of the plate and the multiple reflections from the boundaries in combination with light damping create an incoherent field. Therefore, the total energy density and intensity can be obtained from a linear superposition of the partial energy

density and intensity for the incoherent wave field [2,42,43]. Thus,

$$\langle \underline{e} \rangle = \langle \underline{e}_x \rangle + \langle \underline{e}_y \rangle = \frac{D}{2}\left[\gamma_{x1}^4 (A_x^2 e^{-(\eta/2)\gamma_{x1}x} + B_x^2 e^{(\eta/2)\gamma_{x1}x}) + \gamma_{y1}^4 (A_y^2 e^{-(\eta/2)\gamma_{y1}y} + B_y^2 e^{(\eta/2)\gamma_{y1}y})\right], \tag{26}$$

$$\langle \vec{\underline{I}} \rangle = \langle \underline{I}_x \rangle \vec{i} + \langle \underline{I}_y \rangle \vec{j} = D\omega\left[\gamma_{x1}^3 \left(A_x^2 e^{-(\eta/2)\gamma_{x1}x} - B_x^2 e^{(\eta/2)\gamma_{x1}x}\right)\vec{i} + \gamma_{y1}^3 \left(A_y^2 e^{-(\eta/2)\gamma_{y1}y} - B_y^2 e^{(\eta/2)\gamma_{y1}y}\right)\vec{j}\right]. \tag{27}$$

By observing the similarities between Eqs. (26) and (27), a relationship between the energy density and the intensity is derived:

$$\langle \vec{\underline{I}} \rangle = -\frac{(c_g)_{eff}^2}{\eta\omega} \nabla \langle \underline{e} \rangle, \tag{28}$$

where $(c_g)_{eff} = 2 * \sqrt[4]{(D/m_{eff})\omega^2}$, is defined as the effective group velocity of plate under heavy fluid loading. The EFEA differential equation for a plate is derived by considering a power balance at the steady state over a differential control volume of the plate [41]:

$$\langle \underline{\Pi}_{in} \rangle = \langle \underline{\Pi}_{diss} \rangle + \nabla \langle \vec{\underline{I}} \rangle, \tag{29}$$

Where $\langle \underline{\Pi}_{diss} \rangle$ is the time and space averaged dissipated power. A relationship similar to the one for the dissipated acoustic energy density can be derived for the flexural energy density of the plate:

$$\langle \underline{\Pi}_{diss} \rangle = \eta\omega \langle \underline{e} \rangle. \tag{30}$$

Substituting Eqs. (28) and (30) into Eq. (29) results in the EFEA governing differential equation for the plate under heavy fluid loading:

$$-\frac{(c_g)_{eff}^2}{\eta\omega} \nabla \langle \underline{e} \rangle + \eta\omega \langle \underline{e} \rangle = \langle \underline{\Pi}_{in} \rangle. \tag{31}$$

Compared to the EFEA governing differential equation in vacuum [25], the effective group velocity instead of the normal group velocity and the total damping factor instead of the structural damping factor are used in Eq. (31). The modifications originate from the heavy fluid effects. A finite element formulation [25] is employed for solving Eq. (31) numerically.

### 3.2. Power transfer coefficients for plates under fluid loading

The energy density is discontinuous at connections between members. A joint matrix derived from the power transfer coefficients is utilized for coupling the energy density variables across a joint. The power transfer coefficients are evaluated from analytical solutions of semi-infinite members that demonstrate the same structural characteristics with the components for which the power transfer coefficients are computed. The method developed by Langley and Heron [44] for computing the power transfer coefficients between dry plates is expanded in order to include the fluid loading effects in the derivation of the power transfer coefficients.

A general junction of $N$ semi-infinite plates with some plates in contact with a dense fluid is depicted in Fig. 3(a). The position of the $j$th pate is defined by the angle $\theta_j$, which is the angle

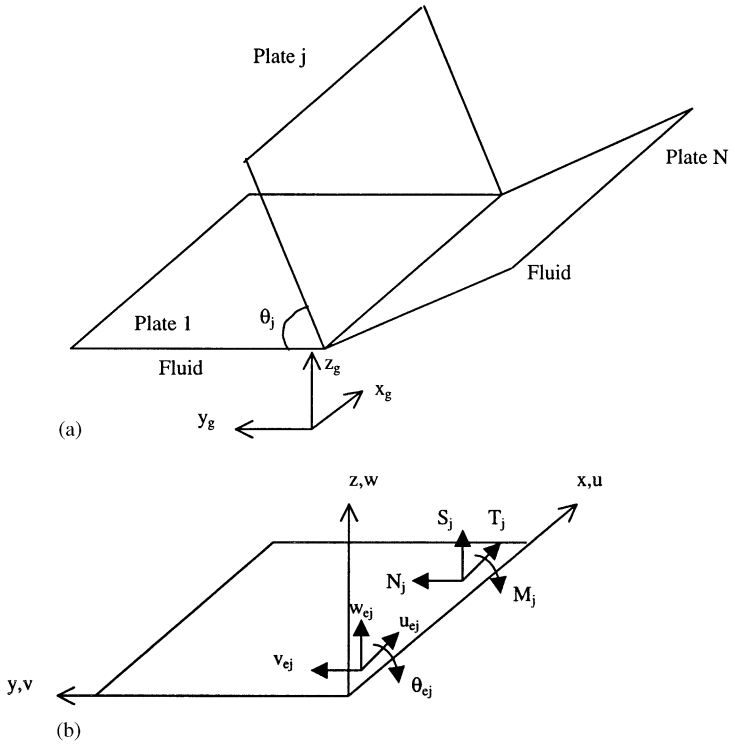


Fig. 3. (a) A general $N$-plate junction with some plates in contact with dense fluid on one side; (b) co-ordinate system, displacement and tractions for plate $j$.

between the global $z$-axis and the local $z$-axis. The in-plane displacements ($u$, $v$) and flexural displacement ($w$) of each plate are related by the compatibility condition at the junction. The displacements $(u, v, w)$ of each plate are defined with respect to a local co-ordinate system $(x, y, z)$. The governing differential equations of motion for the jth plate are:

$$D_j \nabla^4 w + m_j \frac{\partial^2 w}{\partial t^2} = \begin{cases} 0, & \text{without fluid loading,} \\ -p_{z=0}, & \text{with fluid loading,} \end{cases} \tag{32}$$

$$\frac{E_j h_j}{1-v_j^2}\frac{\partial^2 u}{\partial y^2} + \frac{E_j h_j}{2(1+v_j)}\frac{\partial^2 u}{\partial x^2} + \frac{E_j h_j}{2(1-v_j)}\frac{\partial^2 v}{\partial x \partial y} - m_j \frac{\partial^2 u}{\partial t^2} = 0, \tag{33}$$

$$\frac{E_j h_j}{1-v_j^2}\frac{\partial^2 v}{\partial y^2} + \frac{E_j h_j}{2(1+v_j)}\frac{\partial^2 v}{\partial x^2} + \frac{E_j h_j}{2(1-v_j)}\frac{\partial^2 u}{\partial x \partial y} - m_j \frac{\partial^2 v}{\partial t^2} = 0, \tag{34}$$

where $D_j$ is the flexural rigidity, $m_j$ the mass per unit area, $E_j$ the Young's modulus, $v_j$ the poisson ratio and $h_j$ the plate thickness. The fluid loading affects only the bending governing differential equation. The structural damping is neglected in the derivation of the power transfer coefficients. The displacement and the corresponding tractions that act at the edge of a plate at a joint are

presented in Fig. 3(b). Vector $\mathbf{F} = (F_x, F_y, F_z, M)^{\mathrm{T}}$ represents the resultant force and bending moment per unit length along the edge of the joint between all the plates, and $\mathbf{F}_j = (T_j, N_j, S_j, M_j)^{\mathrm{T}}$ represents the tractions which act at the edge of plate $j$ at the joint. $\mathbf{F}$ can be computed by summing $\mathbf{F}_j$ in the form

$$\mathbf{F} = \sum_{j=1}^{N} R_j \mathbf{F}_j, \tag{35}$$

where the transformation matrix $R_j$ is equal to

$$R_j = \begin{pmatrix} 1 & 0 & 0 & 0 \\ 0 & \cos\theta_j & -\sin\theta_j & 0 \\ 0 & \sin\theta_j & \cos\theta_j & 0 \\ 0 & 0 & 0 & 1 \end{pmatrix} \tag{36}$$

In addition, the displacement $\boldsymbol{a} = (u, v, w, \theta)$ of the joint in the global co-ordinate system, and the displacement $\boldsymbol{b}_j = (u_{ej}, v_{ej}, w_{ej}, \theta_{ej})$ of the edge of the plate $j$ in the local co-ordinate system, satisfy the compatibility conditions

$$\mathbf{b}_j = R_j^{\mathrm{T}} \mathbf{a}, \tag{37}$$

where $R_j$ is given in Eq. (36). Eqs. (32)–(37) are used to derive the power transfer coefficients for the joint between the plates. An incident wave is considered to propagate towards the joint in one of the plates. At the joint the wave is partly reflected in the incident plate and partly transmitted to all of the other plates. Considering the space/time dependency of the incident wave as $\exp(-\mathrm{i}kx + \mathrm{i}\mu y + \mathrm{i}\omega t)$, the compatibility at the junction implies that the response in all the plates must have the dependency of $\exp(-\mathrm{i}kx + \mathrm{i}\omega t)$. The dependency with respect to the $y$ coordinate is determined from the plate equations of motion. Assuming that the bending displacement of plate $j$ has a $y$ dependency of $\exp(\mu_f y)$, Eq. (32) implies that $\mu_f$ must satisfy the equation

$$\mu_f^2 = \begin{cases} k^2 \pm k_f^2, & \text{without fluid loading,} \\ k^2 \pm \gamma^2, & \text{with fluid loading,} \end{cases} \tag{38}$$

where $k_f$ and $\gamma$ are defined in Section 2. Therefore, the bending response can be expressed as

$$w = \sum_{n=1}^{2} \alpha_{fn} \exp(-\mathrm{i}kx + \mu_{fn} y + \mathrm{i}\omega t), \tag{39}$$

where $\alpha_{f1}$ and $\alpha_{f2}$ are the amplitudes of the bending response, $\mu_{f1}$ and $\mu_{f2}$ are two valid roots of Eq. (42) and depend on the relative values of $k$ and $k_f$ or $k$ and $\gamma$. Since the equations of the in-plane motion are not modified by the heavy fluid loading, the expression of the in-plane response is the same as the one presented in Ref. [44]:

$$\begin{pmatrix} u \\ v \end{pmatrix} = \left\{ \alpha_L \begin{pmatrix} k \\ \mathrm{i}\mu_L \end{pmatrix} \mathrm{e}^{\mu_L y} + \alpha_S \begin{pmatrix} \mathrm{i}\mu_S \\ -k \end{pmatrix} \mathrm{e}^{\mu_S y} \right\} \exp(-\mathrm{i}kx + \mathrm{i}\omega t), \tag{40}$$

where $\alpha_L$, $\alpha_S$ are the amplitudes of the bending response, $\mu_{f1}$ and $\mu_{f2}$ are two roots computed by Eqs. (33) and (34). Thus, the equation that determines the global displacement of the common

edge is derived according to Ref. [44]:

$$\left\{\sum_{j=1}^{N} R_j K_j R_j^{\mathrm{T}}\right\}\mathbf{a} = R_m \mathbf{f}_m, \tag{41}$$

where $K_j$ is defined as the dynamic stiffness matrix and subscript "$m$" identifies the plate that carries the incident wave. The power transfer coefficients are derived from the following procedure. The edge displacement of each individual plate $(u_{ej}, v_{ej}, w_{ej}, \theta_{ej})$ is recovered from Eq. (37). The amplitude of the bending and the in-plane components of the response $(\alpha_{f1}, \alpha_{f2}, \alpha_L, \alpha_S)$ are computed from the edge displacement field. The wave transmitted to each plate is determined by the imaginary parameters $(\mu_{f1}, \mu_{f2}, \mu_L, \mu_S)$, which govern the $y$ dependency of the transmitted response and the transmitted heading angle is computed as $\phi_r = \cos^{-1}(k/k_r)$, where $r$ can be any of the subscripts $f$, $L$ or $S$. Finally, the magnitude of the power of each propagating wave is calculated by the expressions

$$P_f = (\rho_j \omega^3 \alpha_f^2 / k_B)\sin\phi, \quad P_L = \tfrac{1}{2}\rho_j \omega^3 k_L \alpha_L^2 \sin\phi, \quad P_S = \tfrac{1}{2}\rho_j \omega^3 k_s \alpha_S^2 \sin\phi. \tag{42}$$

The power transfer coefficients associated with each generated wave are calculated as the ratio between the power of the generated wave over the power of the wave incident to the joint. The complete set of transmission coefficients for a joint is written in the form $[\tau]_{eff}$ where subscript "*eff*" indicates that the heavy fluid loading effect is included in the derivation. The joint matrices in the EFEA formulation define the power transfer across elements at the joints and are derived from the power transfer coefficients [26]

$$[J]_{eff} = ([I] - [\tau]_{eff})([I] + [\tau]_{eff})^{-1} \int_B \phi_i \phi_j \mathrm{d}B, \tag{43}$$

where $\phi_i$, $\phi_j$ are Lagrangian basis functions, and $B$ is the boundary area between elements $i$ and $j$ at the joint. Thus, the fluid loading effects are finally included in the derivation of the joint matrices and in the power transfer mechanism in the EFEA system of equations. The final system of EFEA equations is obtained from Eqs. (31) and (43):

$$[[E]_{eff} + \sum [J]_{eff}]\{<\underline{e}>\} = \{f\}, \tag{44}$$

where $[E]_{eff}$ is the system matrix derived from left-hand side of Eq. (31), $\{f\}$ is the vector related to input power in Eq. (31), and $\Sigma$ indicates the addition of the joint matrices that correspond to all the joints in the model to the EFEA system matrix $[E]_{eff}$.

## 4. Validation

In order to validate the new EFEA formulation that includes fluid loading effects in the computations, EFEA results are compared to classical techniques such as the SEA and the modal decomposition method for bodies of revolution. An implementation of the azimuthal modal decomposition method combined with a high order structural finite element and infinite finite elements in the radial direction (SONAX [45]) is utilized in the validation. Comparison of the EFEA results with data from a very dense conventional FEA model is also utilized in the

validation. A flat plate in contact with water from one side, a cylindrical structure immersed in water and a small undersea vehicle are analyzed.

### 4.1. A plate in contact with water from one side

The dynamic response of a thin steel plate with free edge boundary conditions, exposed to a half-space of water, and excited by a time-harmonic point force applied at its center is analyzed (Fig. 4). A similar problem has been analyzed in the past for investigating the effect of fluid loading on plate vibration [46]. The results from the EFEA analysis are compared to the conventional FEA method. The virtual mass method in MSC/NASTRAN [32] is used for the FEA analysis. Since the fluid is assumed to be incompressible in the virtual mass method, only the added mass effect is captured by the FEA analysis. In order to include the radiation damping in the FEA analysis, the frequency-dependent radiation damping factors are computed by Eq. (22) and added to the structural damping of the FEA model. Energy parameters are derived from the discrete vibration computed by the FEA in order to compare the results to the EFEA. The comparison between the two methods is performed at a high enough frequency in order for the EFEA computations to be meaningful. Thus, the FEA model contains a large number of elements in order to provide reliable results at high frequency.

The dimensions of the plate are $0.455\,\mathrm{m} \times 0.375\,\mathrm{m}$ and its thickness is 1 mm. The amplitude of the external force is 1 N, and the material properties for the plate and the water are listed in Tables 1 and 2, respectively. Analyses are performed for all the $\frac{1}{3}$ octave bands between 100 and

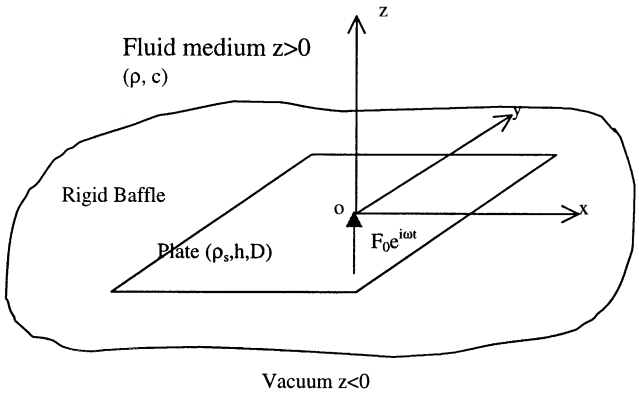


Fig. 4. A rectangular thin elastic plate exposed to heavy fluid loading from one side with time-harmonic point force excitation at the center.

Table 1
Material properties of the rectangular plate

| | |
|---|---|
| Young's modulus (pa) | 2.07E + 11 |
| Density (kg/m$^3$) | 7800.0 |
| The Poisson ratio | 0.333 |
| Damping loss factor | 0.01 |

Table 2
Properties of the fluid medium (water)

| | |
|---|---|
| Density (kg/m$^3$) | 1000.0 |
| Sound speed (m/s) | 1500.0 |

4000 Hz. Since the coincidence frequency of the plate is about 220 kHz, the frequency range analyzed is far below the coincidence frequency. The FEA model utilizes 3000 elements. FEA results are computed at frequency intervals of $\sim$4 Hz. In order to produce energy variables from the FEA analyses, the discrete vibration is utilized for computing the space averaged flexural energy density for the plate. The FEA results for the energy density are frequency averaged for each $\frac{1}{3}$ octave frequency band. The radiation damping factors are added to the structural damping in the FEA analyses. The EFEA model is utilized 100 elements and the external input power defines the excitation for each $\frac{1}{3}$ octave band. The input power can be expressed as

$$P_{in} = \tfrac{1}{2}\mathrm{Re}(FV^*) \quad \text{or} \quad P_{in} = \tfrac{1}{2}|F|^2\mathrm{Re}(A_f), \tag{45}$$

where $F$ is the external applied force, $V^*$ is the conjugate of the velocity of the driving point, and $A_f$ is the admittance at the driving point. Two approaches are utilized for computing the input power. First, the vibration at the driving point computed by the FEA with the specified radiation damping model is employed in Eq. (45) for evaluating the power input into the system. As an alternative, the driving point admittance of an infinite plate derived by the classical technique [12] is employed in Eq. (45) for estimating the input power. Approximating the admittance of a finite system with the admittance of an infinite system is typical for high-frequency analyses [47]. The equation for the driving point admittance below the coincidence frequency is [12]

$$A_f = \left(\frac{1}{8(\rho_s h D)^{1/2}}\right)\frac{4}{5}\left(\frac{k}{\nu k_f}\right)^{2/5}\left(1 - \mathrm{i}\,\tan\frac{\pi}{10}\right), \quad f << f_c, \tag{46}$$

where $\nu = \rho k/(\rho_s h k_f^2)$. The input power by the FEA method and the input power evaluated by the classical technique of driving point admittance of an infinite thin plate under fluid loading are presented in Fig. 5. Good correlation between these two methods indicates that the input power which is computed based on the radiation damping model utilized in this work agrees well with the input power predicted by the classical solution. Then, the frequency averaged input power computed by the FEA method is utilized in the EFEA computations. The mean quadratic velocity computed by the EFEA formulation and FEA method are presented in Fig. 6. The FEA and EFEA results correlate well, particularly in the frequency range between 315 Hz and 2000 Hz. For frequencies beyond this range, differences occur because either the EFEA does not capture the low-frequency dynamic response well or because the FEA method does not capture accurately the high-frequency vibration. The good correlation between the FEA and EFEA results demonstrates that the effective mass effect due to fluid loading is captured correctly in the EFEA equations and in the corresponding numerical implementation.

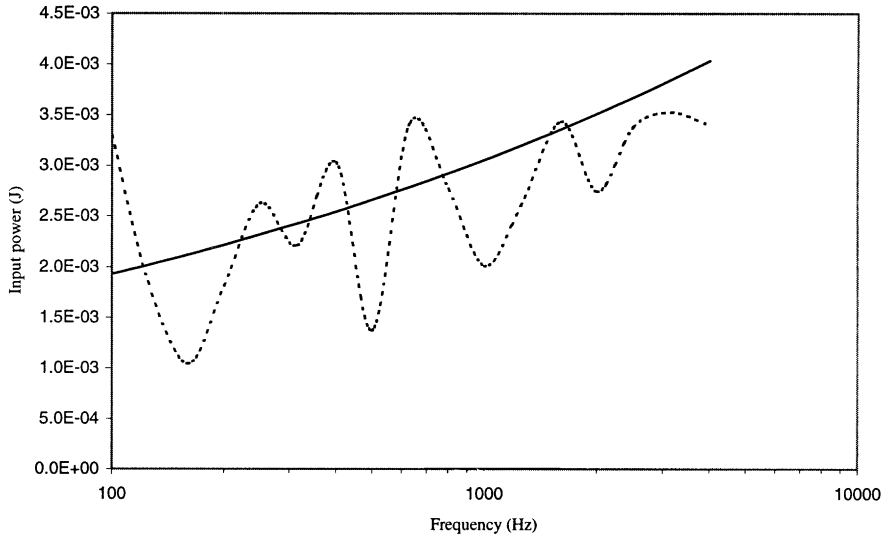


Fig. 5. Input power computed by a classical technique and by the FEA method with the radiation model utilized in this work: ——, classical technique; ------, FEA with specified radiation model.

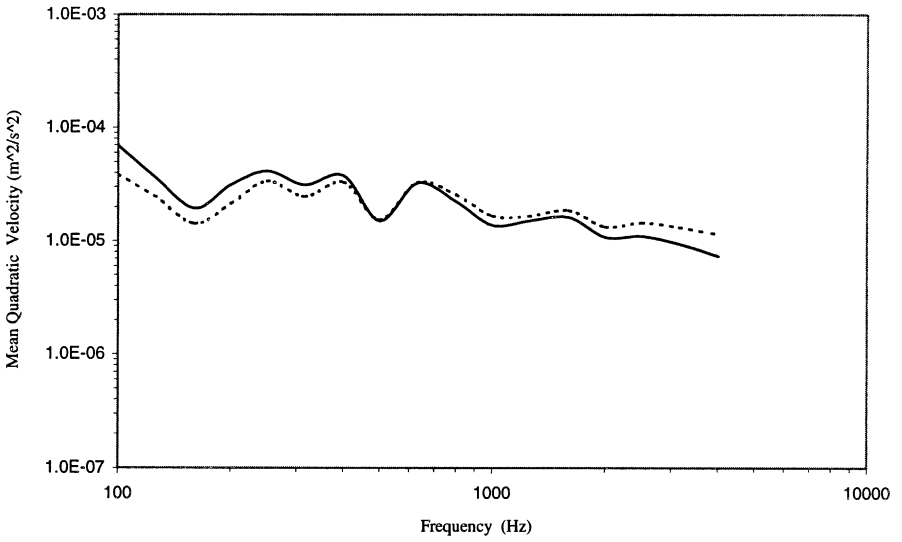


Fig. 6. Comparison of the mean square velocity response of the free rectangular plate under heavy fluid loading: ——, EFEA; -------, dense FEA.

### 4.2. *A cylindrical structure immersed into water*

A cylindrical structure immersed in water is analyzed by the new EFEA formulation. Two common approximations for high-frequency vibration of cylindrical structures are adopted here. The vibrational behavior of the cylindrical structure is considered generally governed by the closely spaced flexural resonance [48,49]. The dispersion relation for a particular waveguide mode

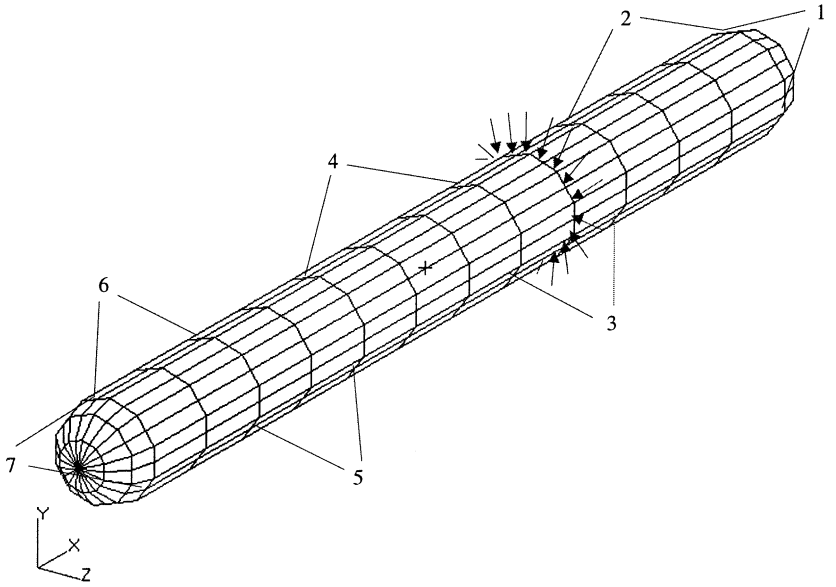


Fig. 7. Energy finite element model of the cylinder.

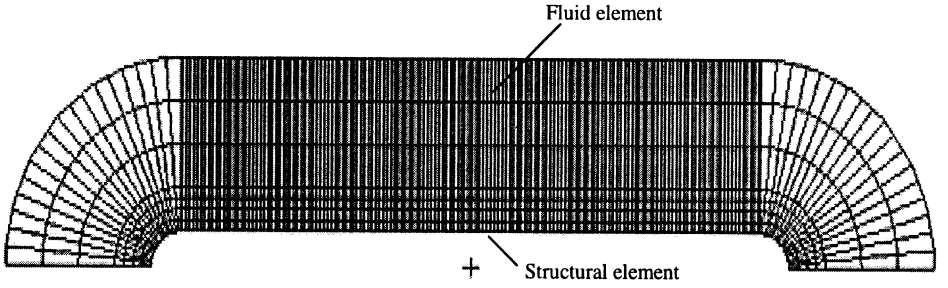


Fig. 8. Axisymmetric finite element model of the cylinder.

and the general behavior of the fluid loading for the cylindrical geometry are considered to be similar to the planar case [49–51]. The curved surface of the cylinder is modelled by sections of flat plate EFEA elements connected at appropriate angles. The coupling among the in-plane and flexural energy densities of connected sections of elements are accounted by the joint formulation. The model for the EFEA formulation is presented in Fig. 7, and is comprised of 360 elements and 300 joints. For comparison, the structure is also analyzed by SONAX [45]. The axisymmetrical SONAX model (Fig. 8) contains 269 structural elements, 538 interface elements, and 1883 fluid elements. The thickness of the structure is 5 mm, the length is 6.6 m, and the inner diameter is 0.6 m. The material properties for the structure and the surrounding acoustic medium are listed in Tables 1 and 2. The coincidence frequency for a plate with similar properties is about 45 kHz. In order to process and compare the results the structure is divided into seven components (Fig. 7). An axisymmetric excitation is applied in the middle of component 3. Analyses are performed over the $\frac{1}{3}$ octave bands from 500 to 1600 Hz. Both methods are expected to provide results valid for comparison over the frequency range 1000 to 1600 Hz. EFEA analyses are performed at lower

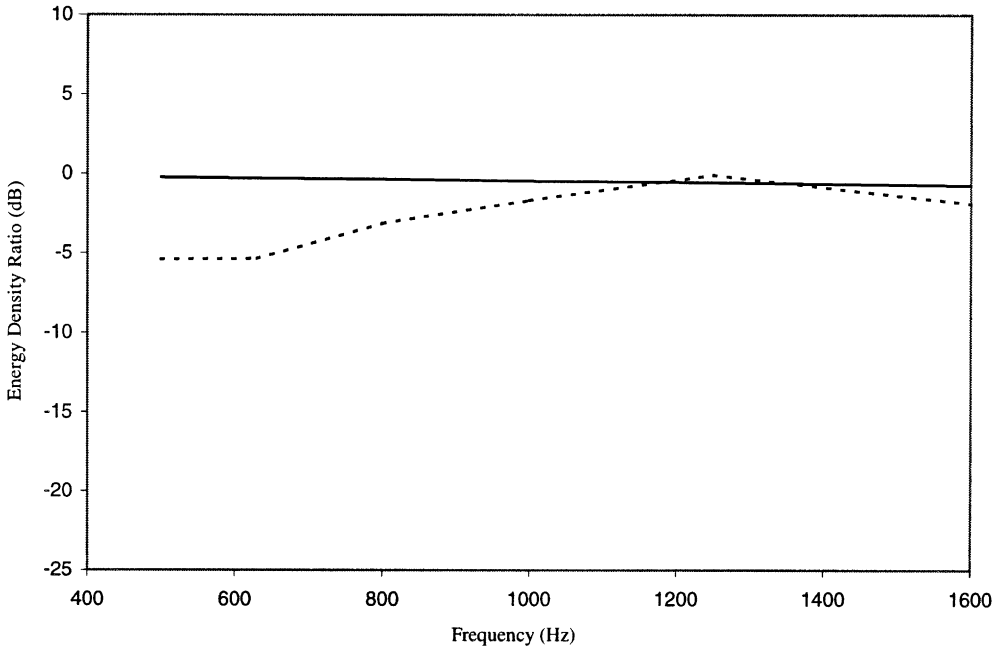


Fig. 9. Bending energy density ratio between part 2 and part 3: ——, EFEA; ------, axisymmetrical FEA.

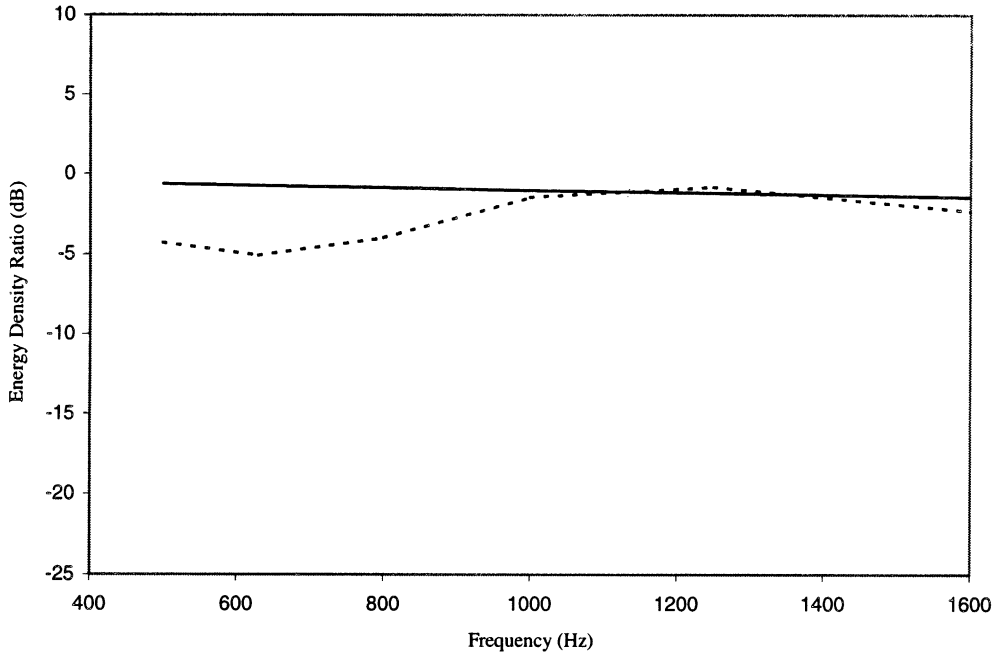


Fig. 10. Bending energy density ratio between part 4 and part 3: ——, EFEA; ------, axisymmetrical FEA.

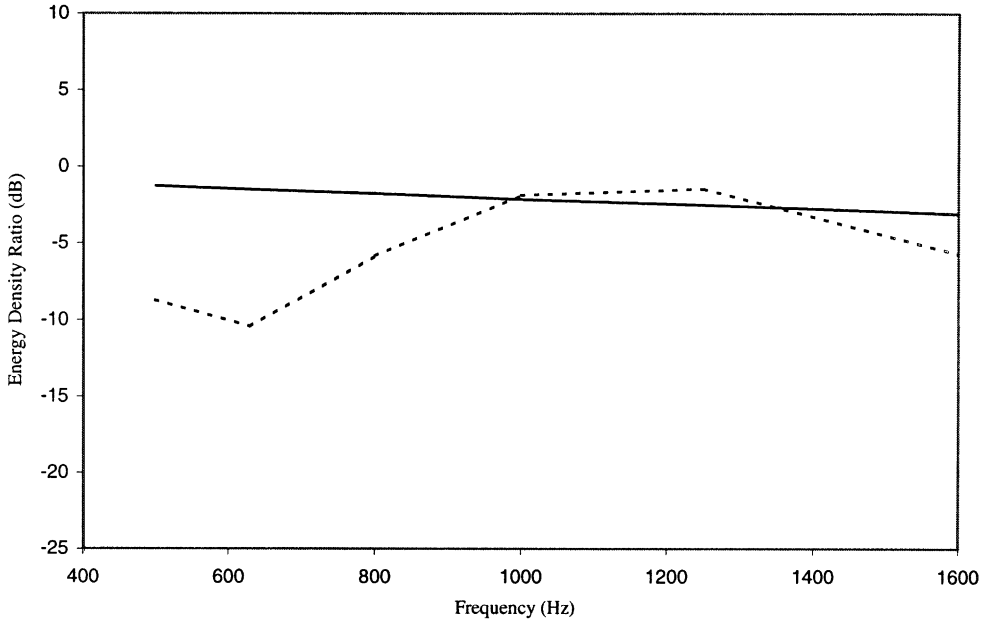


Fig. 11. Bending energy density ratio between part 5 and part 3: ——, EFEA; ------, axisymmetrical FEA.

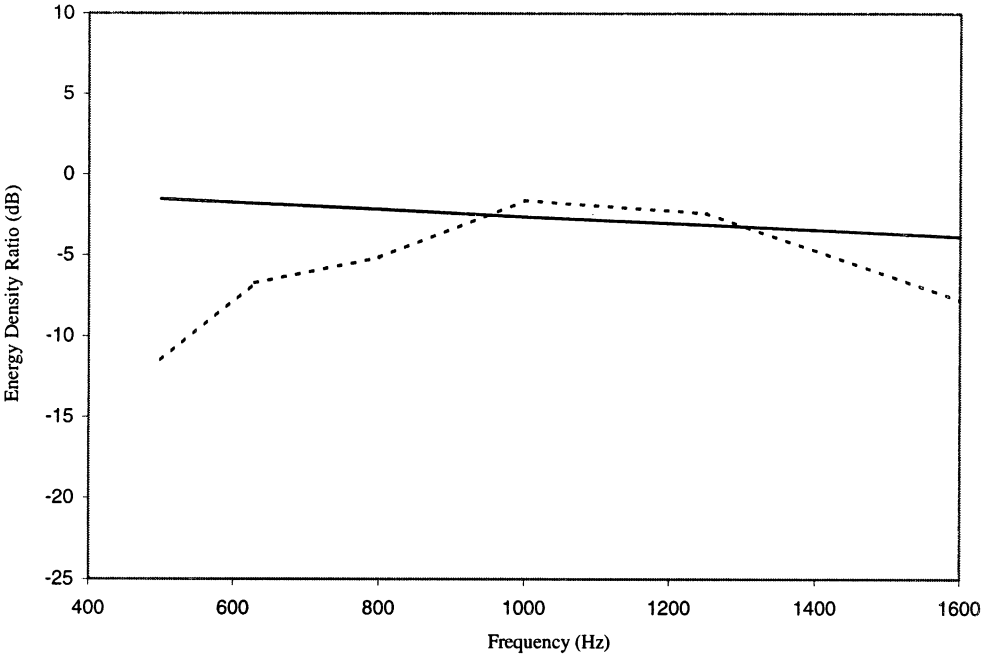


Fig. 12. Bending energy density ratio between part 6 and part 3: ———, EFEA; ------, axisymmetrical FEA.

frequencies in order to demonstrate the inability of the high-frequency method to capture the structural vibration at low frequencies. The flexural energy density ratios between the receiving and the externally excited component are computed by both methods. FEA analyses are performed at $\sim 5$ Hz frequency intervals. The FEA results are frequency averaged over each $\frac{1}{3}$ octave in order to be compared properly with the EFEA results. Results for the four cylindrical components are presented in Figs. 9–12. The two end caps do not include enough wavelengths within their dimension in order to be properly analyzed by EFEA, thus the corresponding results are not considered. The effect of the heavy fluid loading is accounted in both methods. In EFEA the fluid loading is accounted through the added mass, the radiation damping, and in the derivation of the power transfer coefficients, while the SONAX software is based on an azimuthal modal decomposition method combined with structural, fluid and infinite fluid finite elements. The results demonstrate reasonable correlation between the two methods. This is an indication that all of the fluid loading effects are accounted and implemented properly in the EFEA formulation.

### 4.3. A small undersea vehicle

In order to further validate the EFEA developments, a small undersea vehicle is analyzed by the EFEA formulation, the SEA method, and SONAX. The models for the three analyses are presented in Figs. 13–15, respectively. The vehicle is 6 m long and the maximum inner diameter is 0.524 m. The thickness of the vehicle skin is 1 cm, and all four bulkheads have the same thickness 2.54 cm. The EFEA model is comprised by 1060 elements and 600 joints. The SEA model includes 10 subsystems. The SONAX model contains 285 structural elements, 486 interface elements, and 3645 fluid elements. The fluid material is listed in Table 2 and the materials of the structure is listed in Table 3. The coincidence frequency for a flat plate with similar material properties is about 23 kHz. The high-frequency approximation stated in the analysis of the cylindrical structure

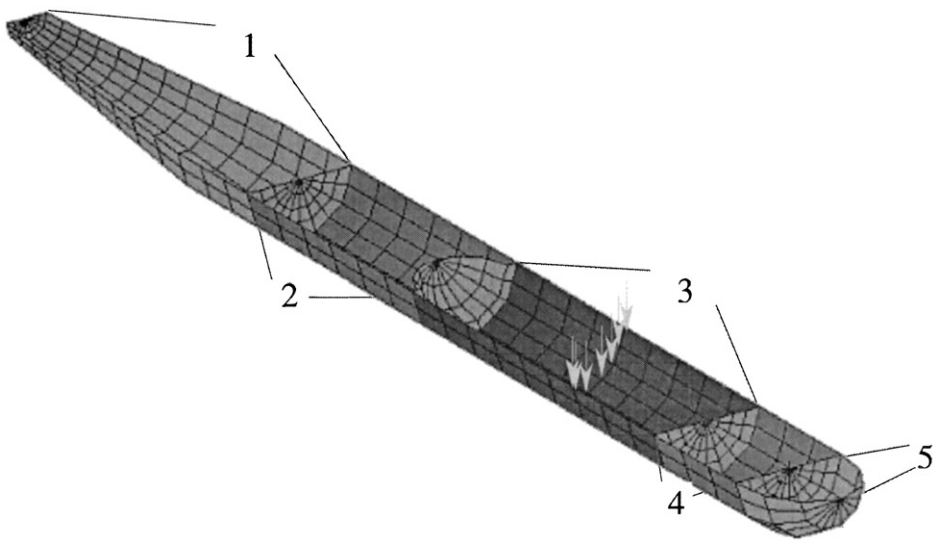


Fig. 13. Energy finite element model of the small undersea vehicle.

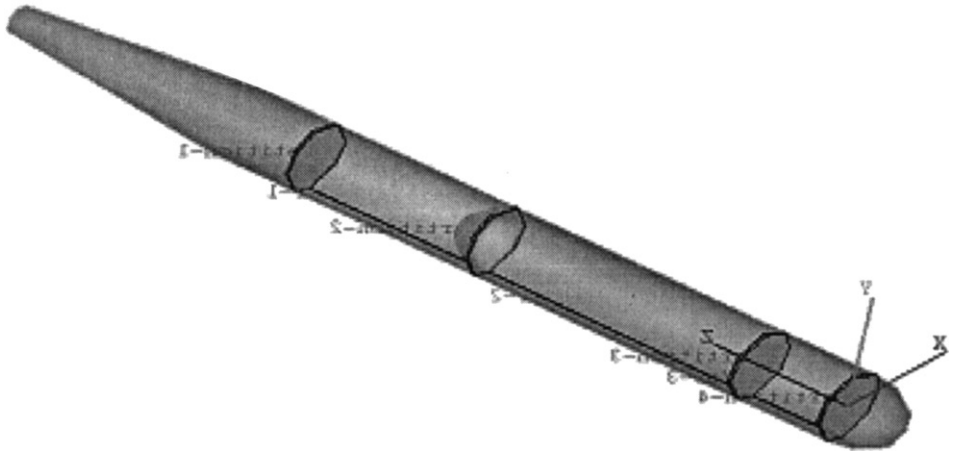

Fig. 14. SEA model of the small undersea vehicle.

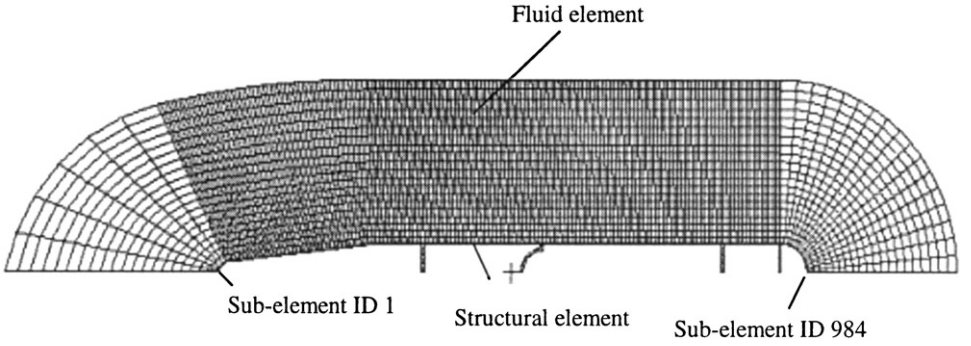


Fig. 15. Axisymmetrical finite element model of the small undersea vehicle.

Table 3
Material properties of the small undersea vehicle

| | |
|---|---|
| Young's modulus (pa) | 7.0E + 10 |
| Density (kg/m$^3$) | 2800.0 |
| The Poisson ratio | 0.3 |
| Damping loss factor | 0.01 |

are considered applicable to the current analysis. The vehicle is divided into five components by the four bulkheads (Fig. 13) and an axisymmetric excitation is applied in the middle of component 3. Analyses are performed over the $\frac{1}{3}$ octave bands between 500 and 4000 Hz. In order to identify a frequency range where the two high-frequency methods (EFEA and SEA) are expected to provide similar results to the SONAX solution, the profile of the vibration along the length of the vehicle is presented in Fig. 16 for three different frequencies. It can be observed that only from $\sim$1500 Hz and above there are enough wavelengths in the structure for the high-frequency methods to be valid. It is also demonstrated that the near field response in the vicinity of the excitation is

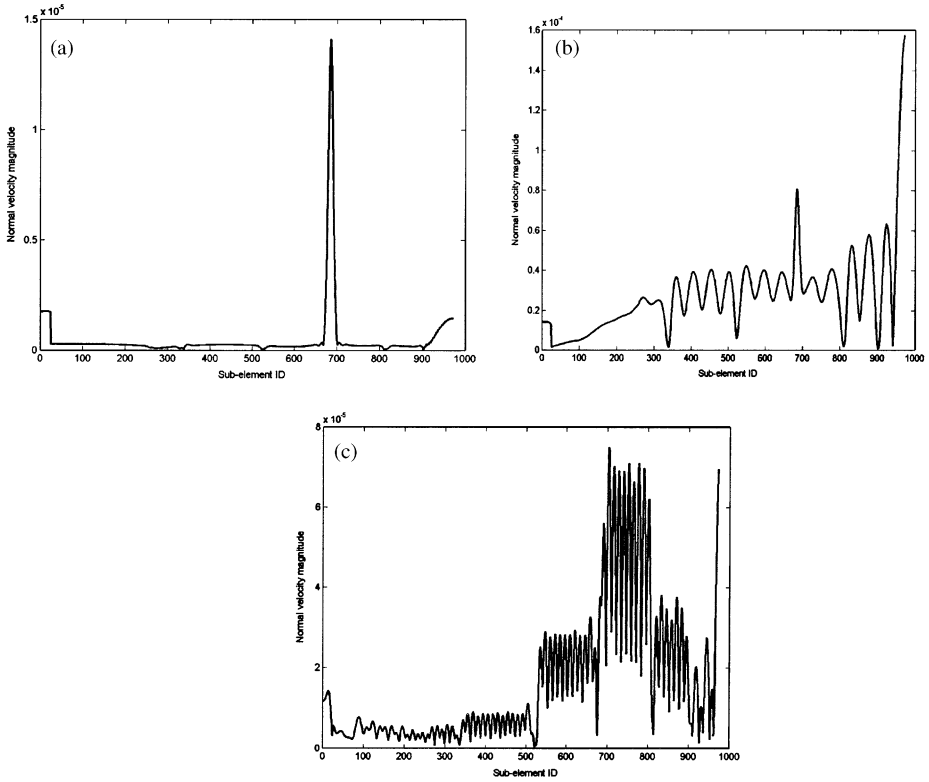


Fig. 16. Vibration profile along the length of the vehicle at three frequencies: (a) 500 Hz, 1413 Hz, (c) 3548 Hz.

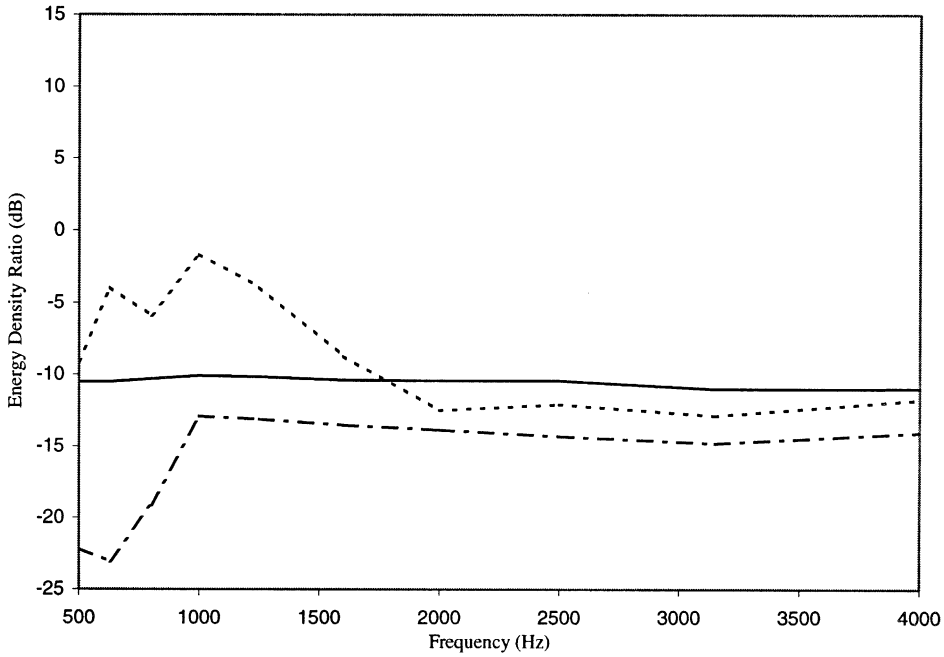


Fig. 17. Energy density ratio between part 1 and part 3: ——, EFEA; ------, axisymmetrical FEA; - · · · -, SEA.

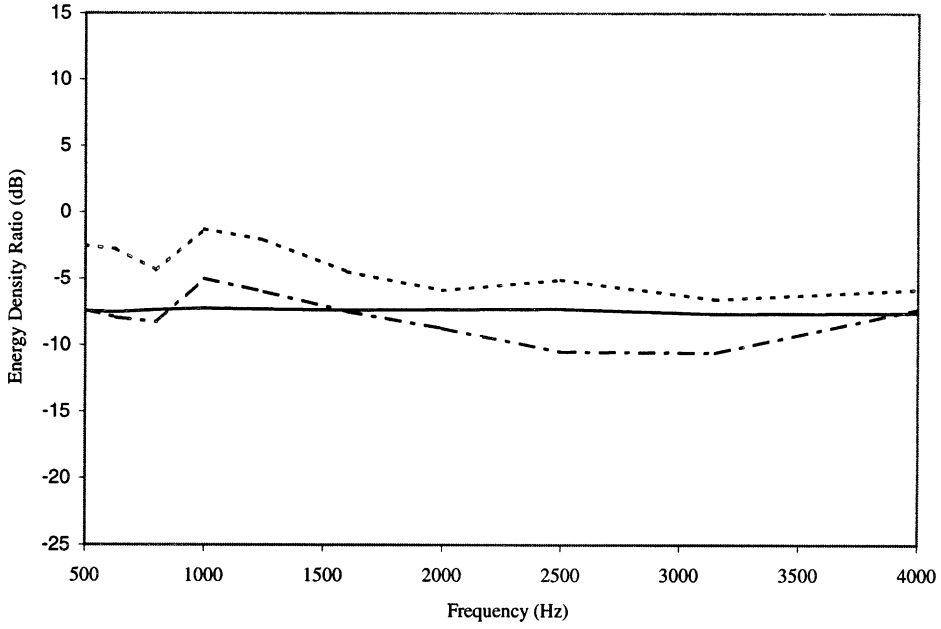


Fig. 18. Energy density ratio between part 2 and part 3: ——, EFEA; -------, axisymmetrical FEA; - · - · -, SEA.

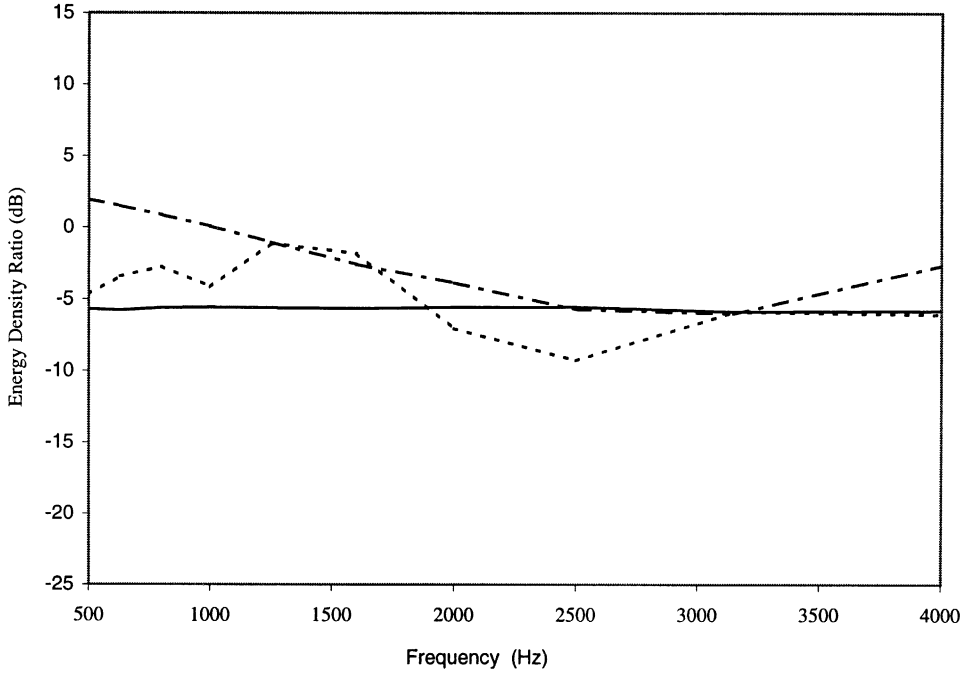


Fig. 19. Energy density ratio between part 4 and part 3: ——, EFEA; -------, axisymmetrical FEA; - · - · -, SEA.

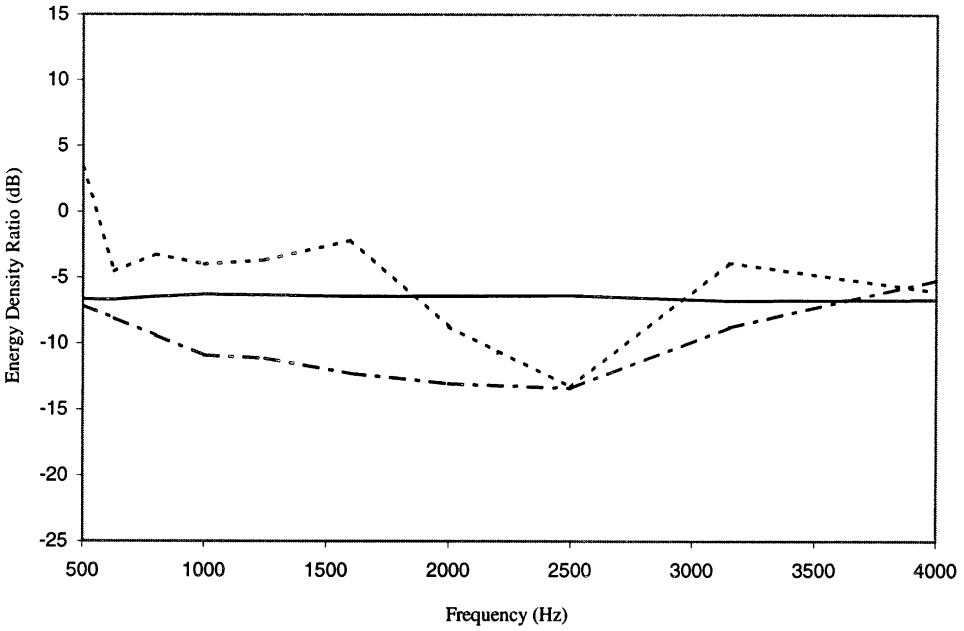


Fig. 20. Energy density ratio between part 5 and part 3: ——, EFEA; ------, axisymmetrical FEA; - · - · -, SEA.

negligible at high frequency since many modes are contributing to the vibrational field. Results for the energy density ratio between the four cylindrical components and the component where the excitation is applied are presented in Figs. 17–20. The results demonstrate good correlation between the three methods at the frequency above 1500 Hz. Several advantages are associated with the new EFEA formulation. The computational time is much reduced compared to a SONAX analysis at high frequencies. Specially for one $\frac{1}{3}$ octave frequency the total CPU time for SONAX on Sun Ultra 10 workstation was $\sim$2000 s while the EFEA computation required $\sim$120 s on a personal computer with Pentium III. The variation of the energy distribution within each component can be computed by EFEA. This constitutes an improvement over the lumped parameter SEA method. The external input power and the damping treatment can be applied at a local level in EFEA, while the SEA method considers these parameters distributed equally over an entire subsystem. Therefore, the new EFEA formulation provides an improved method for high-frequency vibration of plates under heavy fluid loading.

## 5. Conclusions

An EFEA formulation for analyzing the high-frequency vibration of thin elastic plates in contact with dense fluid is presented. The added mass and the radiation effects are included in the derivation of the EFEA governing differential equation. The fluid loading effect is also accounted for in the derivation of the power transfer coefficients and the derivation of the joint EFEA matrices. The new EFEA formulation and its implementation are validated by comparing EFEA

results to solutions obtained by very dense conventional FEA models and results obtained by classical solutions such as the SEA and the modal decomposition method. Good correlations are observed between the new EFEA solution and the other established solutions in intermediate frequency ranges where all methods are valid. The advantages of the EFEA formulation are outlined. Overall, it is demonstrated that the new EFEA formulation captures properly the fluid loading effects.

## Acknowledgements

The research presented in this paper was supported by the Office of Naval Research, Code 334, under contract number N00014-00-0382. The authors acknowledge Dr. Luise Couchman and Dr. Terry Bazow for their assistance in obtaining and utilizing the SONAX code. The analysis of the small undersea vehicle was supported by NUWC, Newport under contract number N66604-01-M-2560.

## References

[1] N. Vlahopoulos, L.O. Garza-Rios, C. Mollo, Numerical implementation, validation, and marine applications of an energy finite element formulation, Journal of Ship Research 43 (1999) 143–156.
[2] W. Zhang, A. Wang, N. Vlahopoulos, Validation of the EFEA method through correlation with conventional FEA and SEA results, SAE Noise and Vibration Conference, SAE Paper No. 2001-01-1618, 2001.
[3] W. Zhang, A. Wang, N. Vlahopoulos, An alternative energy finite element formulation based on incoherent orthogonal waves and its validation for marine structures, Finite Elements in Analysis and Design 38 (2002) 1095–1113.
[4] G. Madanik, The influence of fluid loading on the radiation from orthographic plates, Journal of Sound and Vibration 83 (1965) 288–299.
[5] G. Madanik, E.M. Kerwin, Jr., Influence of fluid loading on the radiation from infinite plates below the critical frequency, The Journal of the Acoustical Society of America 40 (1966) 1034–1038.
[6] P.R. Nayak, Line admittance of infinite isotropic fluid-loaded plates, The Journal of the Acoustical Society of America 47 (1970) 191–201.
[7] H.G. Davies, Low frequency random excitation of water-loaded rectangular plates, Journal of Sound and Vibration 15 (1971) 107–126.
[8] H.G. Davies, Sound from turbulent-boundary-layer-excited panels, The Journal of the Acoustical Society of America 49 (1971) 878–889.
[9] D.G. Crighton, Force and moment admittance of plates under arbitrary fluid loading, Journal of Sound and Vibration 20 (1972) 209–218.
[10] B.E. Sandman, Motion of a three-layered elastic-viscoelastic plate under fluid loading, The Journal of the Acoustic Society of America 57 (1975) 1097–1107.
[11] P.W. Smith Jr., Line input admittance of fluid-loaded wave-bearing layers, Journal of Sound and Vibration 48 (1976) 45–46.
[12] D.G. Crighton, Point admittance of an infinite thin elastic plate under fluid loading, Journal of Sound and Vibration 54 (1977) 389–391.
[13] B.E. Sandman, Fluid–loaded vibrations of an elastic plate carrying a concentrated mass, Journal of Acoustic Society of America 61 (1977) 1503–1510.
[14] D.G. Crighton, The free and forced waves on a fluid-loaded elastic plate, Journal of Sound and Vibration 63 (1979) 225–235.

[15] D.G. Crighton, Approximation to the admittance and free wavenumbers of fluid-loaded panels, Journal of Sound and Vibration 68 (1980) 15–33.
[16] D.G. Crighton, G. Maidanik, Acoustic and vibration fields generated by ribs on a fluid-loaded panel I: plane-wave problems for a single rib, Journal of Sound and Vibration 75 (1981) 437–452.
[17] R.F. Kelitie, H. Peng, Acoustic power radiated from point-forced thin elastic plates, Journal of Sound and Vibration 112 (1987) 45–52.
[18] G. Maidanik, Response of ribbed panels to reverberant acoustic fields. The Journal of the Acoustical Society of America 34 (1962) 809–826.
[19] F.G. Leppington, E.G. Broadbent, F.R.S., K.H. Heron, The acoustic radiation efficiency of rectangular panels, Proc. R. Soc. Lond. A 382 (1982) 245–271.
[20] K. Andresen, Underwater noise from ship hulls, Proceedings, International Conference on Noise & Vibration in the Marine Environment, May, London, 1999, pp. 1–22.
[21] M.C. Junger, D. Feit, Sound Structure and Their Interaction, 2nd Edition, MIT press, Cambridge, MA, 1986.
[22] O.M. Bouthier, R.J. Bernhard, C. Wohlever, Energy and structural intensity formulations of beam and plate vibration, Proceedings, International Congress on Intensity Techniques, Senlis, France 1990, pp. 37–44.
[23] O.M. Bouthier, R.J. Bernhard, Models of space-averaged energetics of plates, American Institute of Aeronautics and Astronautics Journal 30 (1992) 34–44.
[24] O.M. Bouthier, Energetics of Vibrating Systems, Ph.D. Dissertation, Mechanical Engineering Department, Purdue University, Lafayette, IN, 1992.
[25] P. Cho, Energy Flow Analysis of Coupled Structures, Ph.D. Dissertation, Mechanical Engineering Department, Purdue University, Lafayette, IN, 1993.
[26] J.E. Huff Jr., R.J. Bernhard, Prediction of high frequency vibrations in coupled plates using energy finite elements, Proceedings, Inter-Noise 95, Newport Beach, CA, USA, 1995, pp. 1221–1126.
[27] D.J. Nefske, S.H. Sung, Power flow finite element analysis of dynamic systems: basic theory and applications to beams, Journal of Vibration, Acoustics Stress and Reliability 220 (1999) 135–154.
[28] R.J. Bernhard, J.E. Huff, Jr., Structural-acoustic design at high frequency using the energy finite element method, Journal of Vibration and Acoustics 121 (1999) 295–301.
[29] M.C. Junger, Approaches to acoustic fluid-elastic structure interactions, Journal of Acoustical Society of America 82 (1987) 1115–1121.
[30] D.G. Crighton, The 1988 Rayleigh Medal Lecture: fluid loading –the interaction between sound and vibration, Journal of Sound and Vibration 133 (1989) 1–27.
[31] D. Lee, R.L. Sternberg, M.H. Schultz (Eds.), Proceedings of the First IMACS Symposium on Computational Acoustics. Computational Acoustics: Algorithms and Applications, Elsevier, Amsterdam, 1988.
[32] D.N. Herting, MSC/NASTRAN, Advanced Dynamics User's Guide, Version 70, MacNeal-Schwendler Corporation, 1997.
[33] ABAQUS/Standard, User's Manual, Version 6.2-1, Hibbitt, Karlsson & Sorensen, 2001.
[34] D.G. Crighton, D. Innes, Low frequency acoustic radiation and vibration response of locally excited fluid-loaded structures, Journal of Sound and Vibration 91 (1983) 293–314.
[35] R. Lyon, Statistical Energy Analysis of Dynamical Systems: Theory and Application, The MIT Press, Cambridge, MA, 1975.
[36] R. Lyon, In-plane contribution to structural noise transmission, Noise Control Engineering Journal 26 (1986) 22–27.
[37] J. Woodhouse, An approach to the theoretical background of statistical energy analysis applied to structural vibration, The Journal of the Acoustical Society of America 69 (1981) 1695–1709.
[38] VibroAcoustic Payload Environment Prediction System (VAPEPS) Manual, Version 5.5, JPL D-9775, Jet Propulsion Laboratory, May 1991.
[39] G. Maidanik, A.J. Tucker, Transmission of free waves across a rib on a Panel, Journal of Sound and Vibration 49 (1976) 445–452.
[40] G. Maidanik, Influence of fluid loading and compliant coating on the coupling loss factor across a rib, Journal of Sound and Vibration 60 (1978) 313–318.
[41] L. Cremer, M. Heckl, E.E. Ungar, Structure-Borne Sound, Springer, Berlin, 1973.

[42] M.N. Ichchou, L. Jezequel, Comments on simple models of the energy flow in vibrating membranes and on simple models of the energetics of transversely vibrating plates, Journal of Sound and Vibration 195 (1996) 679–685.
[43] R.S. Langley, Wave intensity technique for the analysis of high frequency vibration, Journal of Sound and Vibration 159 (1992) 483–502.
[44] R.S. Langley, K.H. Heron, Elastic wave transmission through plate/beam junctions, Journal of Sound and Vibration 143 (1990) 214–253.
[45] T. Bazow, SONAX user's manual, Naval Research Laboratory, Washington DC, 1997.
[46] A. Berry, A new formulation for the vibration and sound radiation of fluid-loaded plates with elastic boundary conditions, The Journal of the Acoustic Society of America 96 (1994) 889–901.
[47] F. Han, R.J. Bernhard, et al., Energy flow analysis of vibrating beams and plates for discrete random excitations, Journal of Sound and Vibration 208 (1997) 841–859.
[48] D.M. Photiadis, B.H. Houston, E.G. Willams, J.A. Bucaro, Resonant response of complex shell structures, Journal of Acoustical Society of America 108 (2000) 1027–1035.
[49] J.F.M. Scott, The free modes of propagation of an infinite fluid-loaded thin cylindrical shell, Journal of Sound and Vibration 125 (1988) 241–280.
[50] D.M. Photiadis, Fluid loaded structures with one dimensional disorder, Applied Mechanics Review 49 (1996) 100–125.
[51] G. Pavic, Vibrational energy flow in elastic circular cylindrical shells, Journal of Sound and Vibration 142 (1990) 293–310.